43rd AIAA Aerospace Sciences Meeting and Exhibit
Reno, NV, January 10-13, 2005

AIAA-2005-0711

EXTINGUISHMENT OF CUP-BURNER FLAMES IN LOW GRAVITY

Fumiaki Takahashi
National Center for Microgravity Research on Fluids and Combustion
NASA Glenn Research Center
Cleveland, OH 44135

Gregory T. Linteris
Fire Research Division, National Institute of Standards and Technology
Gaithersburg, MD 20899

Viswanath R. Katta
Innovative Scientific Solutions Inc.
Dayton, OH 45440

ABSTRACT

The effects of oxidizer stream velocity and oxygen concentration, as well as gravity and pressure, on the extinguishment limits of laminar co-flow diffusion flames of methane, formed in a cup-burner apparatus, have been studied experimentally and computationally. A first attempt was made to measure the cup-burner minimum extinguishing concentration (MEC) of CO_2 in microgravity (μg) aboard the NASA Reduced Gravity Aircraft (KC-135). Numerical simulations with detailed chemistry and radiative heat-loss models were performed to reveal the flame structure during the unsteady blowoff-type extinguishing processes and to predict the extinguishment limits. The MEC values determined for various oxidizing environments were:

	Experiment	Computation
Air/1*g*/1 atm	(15.7 ± 0.6) %	14.5 % (16.1 %)
Air/1*g*/0.7 atm	(15.4 ± 0.5) %	13.5 %
30 % O_2/1*g*/1 atm	(34.0 ± 1.2) %	31.0 %
30 % O_2/1*g*/0.7 atm	(32.4 ± 1.1) %	29.9 %
21 % O_2/μg/1 atm	(21.4 ± 0.7) %	19.1 %

Considering the complex chemistry and flow-field interactions in the blowoff extinguishment processes, the predicted MEC values were consistently in good agreements (~8 % less on average) with the measurements. The relatively high MECs of CO_2 in oxygen-enriched environments point to a need for further trade-off studies of fire-extinguishing agents suitable for spacecraft and surface habitats in space exploration.

INTRODUCTION

To enable NASA's human exploration of the moon and Mars, fire safety for spacecraft and planet surface bases is essential for mission success. NASA's fire safety approach for manned spacecraft has been based primarily upon controlling the flammability of materials onboard and eliminating ignition sources[1-3]. The longer-duration missions for space exploration, however, increase the likelihood of accidental fire events aboard spacecraft or in surface habitats. Incipient or established fires must be promptly detected and extinguished by a fire protection system. To develop effective fire protection systems, the behavior of fires in various environments encountered in the space exploration must be properly understood. Fire behavior and suppression processes in the space exploration missions are strongly influenced by low-gravity environments in flight and on the planetary surfaces. Thus, fire safety technology must be tailored to respond to the unusual fire characteristics in low-gravity environments[1].

The worst case oxygen concentration and pressure environment is currently 30 % oxygen in nitrogen at 70.3 kPa (0.7 atm). This atmosphere corresponds to the Space Shuttle and International Space Station (ISS) environments that are prescribed for crew conditioning prior to extravehicular activities[2,3]. Such an oxygen-enriched atmosphere may also be used for the future spacecraft and habitats in order to reduce the mass of the inert-gas component needed to bring up to space.

Fire-extinguishing agents act to suppress the flame physically and chemically[4,5]. Carbon dioxide (CO_2) and water-based foam used in the ISS as well as numerous terrestrial applications are physically acting

agents. These agents are relatively inefficient as fire suppressants[1-3]. The chemically active agent, halon 1301 (CF_3Br), which is still in use in the Space Shuttle, is highly effective, but its production was banned by the Montreal Protocol[6,7] in 1995. Although the existing systems may continue to be used, new agents or techniques are ultimately needed for long-duration missions[2,3,8]. Physically acting agents, despite their lower effectiveness, are more likely to be used for space applications due to environmental control system and crew safety considerations.

To determine the effectiveness of gaseous fire-extinguishing agents, the cup burner method, specified in national and international standards[9,10], has most widely been used[11-18] in fire safety engineering for terrestrial applications. Therefore, the use of the cup burner apparatus for fire safety in low-gravity space exploration is a logical extension. Vast normal-gravity data bases of the minimum extinguishing concentration (MEC) for a variety of fuels and agents are available for comparison. The cup-burner flame is a laminar co-flow diffusion flame with a circular fuel source (either a liquid pool or a low-velocity gas jet) inside a co-axial chimney with an oxidizing stream. An agent is generally introduced into the coflowing oxidizer in the cup-burner apparatus to determine the MEC of agent. The MEC measured by the cup burner is then used for determining the minimum design concentration of a gaseous agent, along with third-party approval procedures for a complete fire extinguishing system[18].

In recent years, numerical investigations[19-26] using detailed chemistry models have revealed the co-flow diffusion flame structure, blowoff phenomena, and physical and chemical suppression processes. Major findings include a decisive role of the peak reactivity spot (i.e., *reaction kernel*), formed at the flame attachment point in the edge (base) of diffusion flames, in blowoff processes.

The overall objectives of the present study are to understand the physical and chemical processes of cup-burner flame suppression phenomena and to provide rigorous testing of numerical models, which include detailed chemistry and radiation sub-models. This paper describes the experimental and numerical extinguishment limits, as well as the flame structure changes which occur near the limits, for methane as the fuel and CO_2 as the agent in various oxidizing environments relevant to the space exploration missions.

EXPERIMENTAL PROCEDURES

The NASA Reduced Gravity Aircraft (KC-135) hardware for fire suppression in extraterrestrial environments (the FSEE rig), used for both microgravity (μg) and normal earth gravity ($1g$) testing, consists of the experiment rig (Fig. 1a), the support rack (Fig. 1b), and the aircraft gas bottle rack facility for the oxidizer and agent. The experiment rig is a standard 2.2-s Drop Tower "A-frame"-style rig modified for operation on the KC-135. The support rig contains a fuel lecture-bottle, a back-pressure regulator, video equipment, and computer interface.

The standard microgravity cylindrical test chamber (25.5 cm inner diameter × 53.3 cm length, aluminum) has four rectangular (10 cm width × 15 cm height) observation windows. The cup-burner apparatus is coaxially placed inside the test chamber. A cylindrical stainless-steel cup (28 mm i.d., 31 mm o.d., 45º-chamfered inside the rim) is coaxially positioned inside

(a)

(b)

Fig. 1 KC-135 hardware (FSEE). (a) Experiment rig, (b) support rig.

a quartz chimney (85 mm i.d., 45.7 cm height), through which the oxidizer and agent flow. A hot-wire igniter (coiled 29 gauge Kanthal) is used to ignite the fuel. A rotary solenoid, placed underneath the chamber, is used to position the igniter near the burner for ignition and away from it otherwise. To provide uniform flow, two layers of honeycomb plates (1.6 mm cell size, 15 mm thickness, aluminum alloy) and two screens (40 mesh and 100 mesh, stainless steel) atop the honeycomb are placed in the base of the chimney, and a sintered porous plate (3.2 mm thickness, 25 μm to 40 μm pore size, 60 % density, stainless steel) plugs the fuel cup at 6.4 mm below the exit plane. In the aircraft testing, the exhaust from the test chamber is connected to an outboard vent via the back-pressure regulator (Tescom, 44-4700, ER3000*), which maintain the chamber pressure at a set pressure.

Gas flows were measured by mass flow meters (Hastings HFM-300 [fuel and agent], HFM-301 [oxidizer]) which were calibrated so that their uncertainty is 1 % of indicated flow. The fuel gas used is methane (Matheson UHP, 99.97 %) and the fire-extinguishing agent is carbon dioxide (Airgas, 99.99 %). The oxidizers are (21 ± 0.21) % or (30 ± 0.30) % oxygen in nitrogen (AGA, primary standard mixture) for the aircraft tests and house compressed air for the 1*g*-laboratory experiment. The compressed air is filtered, dried, and cleaned to remove aerosols and water vapor.

Prior to the extinguishment test, the flame was lit on for a certain period (~16 minutes) to ensure a thermal steady state for the burner. In the aircraft experiment, the flame was re-ignited during the high-g pull-up period, and the agent was injected during the low-g period. To determine the extinguishment condition, for a fixed methane flow rate, the agent was added (in increments of < 1 % near extinguishment) to co-flowing air (held at a constant flow rate) manually until extinguishment occurred.

The experimental control and data acquisition were achieved by using an onboard computer (Dolch, PAC, Pentium III, 600 MHz) and software written in a graphical programming language (LabVIEW). The oxidizer, fuel, and agent flow-control solenoid valves, the igniter rotary solenoid, and the igniter power were initiated manually through the computer interface. Data signals from the mass flow meters, gas-temperature thermocouples, gas-line and test-chamber pressure transducers, a tri-axis accelerometer (Crossbow, CXL02TG3-S), and a thermopile radiometer (Dexter, ST150 Amplified, nitrogen filled, KRS-5 window) were digitize and recorded at 30 Hz using a data acquisition board (National Instruments, PCI-6033E). The radiometer is placed behind a neutral density filter with its optical axis perpendicularly to the burner axis. The extinguishment process was observed by two CCD color cameras (Hitachi KP-D8 and HV-D30) with orthogonal views and their S-video signals were recorded using two sets of digital video cassette recorders (Sony DVCAM DSR-V10), time-code generators, and video titlers (Horita, TG-50 and SCT-50, respectively).

Reported uncertainties in the experimental data are of Type B, expressed as expanded uncertainties, with a coverage factor of two. The uncertainty in the MEC is 3.4 %, in gas co-flow velocity 3.6 %, and test chamber pressure, 1 %.

NUMERICAL METHODS

A time-dependent, axisymmetric numerical code (UNICORN[27]) is used for the simulation of unsteady jet diffusion flames stabilized on the cup burner. The code solves the axial and radial (*z* and *r*) full Navier-Stokes momentum equations, continuity, and enthalpy- and species-conservation equations on a staggered-grid system. The body-force term due to the gravitational field is included in the axial-momentum equation to simulate upward-oriented flames. A clustered mesh system is employed to trace the gradients in flow variables near the flame surface. A detailed reaction mechanism of GRI-V1.2[28] for methane-oxygen combustion (31 species and 346 elementary reactions) is incorporated into UNICORN. Thermophysical properties of species are calculated from the polynomial curve fits for 300 - 5000 K. Mixture viscosity and thermal conductivity are then estimated using the Wilke and Kee expressions, respectively. A simple radiative heat-loss model[29] based on optically thin-media assumption and Plank-mean absorption coefficients for CO_2, H_2O, CH_4, and CO was incorporated into the energy equation.

The finite-difference forms of the momentum equations are obtained using an implicit QUICKEST scheme[28], and those of the species and energy equations are obtained using a hybrid scheme of upwind and central differencing. At every time-step, the pressure field is accurately calculated by solving all the pressure Poisson equations simultaneously and using the LU (Lower and Upper diagonal) matrix-decomposition technique.

Unsteady axisymmetric calculations for the cup-burner flames are made on a physical domain of 200 × 47.5 mm using a 251 × 101 or 541 × 251 non-uniform

*Certain commercial equipment, instruments, or materials are identified in this paper to adequately specify the procedure. Such identification does not imply recommendation or endorsement by NASA or NIST, nor does it imply that the materials or equipment are necessarily the best available for the intended use.

grid system that yielded 0.2 × 0.2-mm or 0.05 × 0.05-mm minimum grid spacing, respectively, in both the z and r directions in the flame zone. The computational domain is bounded by the axis of symmetry and a chimney wall boundary in the radial direction and by the inflow and outflow boundaries in the axial direction. The boundary conditions are treated in the same way as those reported in earlier papers[22-26]. The outflow boundary in z direction is located sufficiently far from the burner exit (>7 fuel-cup diameters) such that propagation of boundary-induced disturbances into the region of interest is minimal. Flat velocity profiles are imposed at the fuel and air inflow boundaries, while an extrapolation procedure with weighted zero- and first-order terms is used to estimate the flow variables at the outflow boundary.

The cup burner outer diameter is 28 mm and the burner wall is treated as a 1-mm long and 1-mm thick tube. The wall temperature is set at 600 K, which is somewhat higher than the measurement made using a glass cup burner[24]. The fuel and oxidizer velocities are 0.921 cm/s and 10.7 cm/s, respectively. The low fuel velocity represents a condition at which the flame size is comparable to that of typical liquid-fuel cup-burner flames. The air velocity is in the middle of the so-called "plateau region[9,14,16], where the extinguishing agent concentration is independent of the oxidizer velocity.

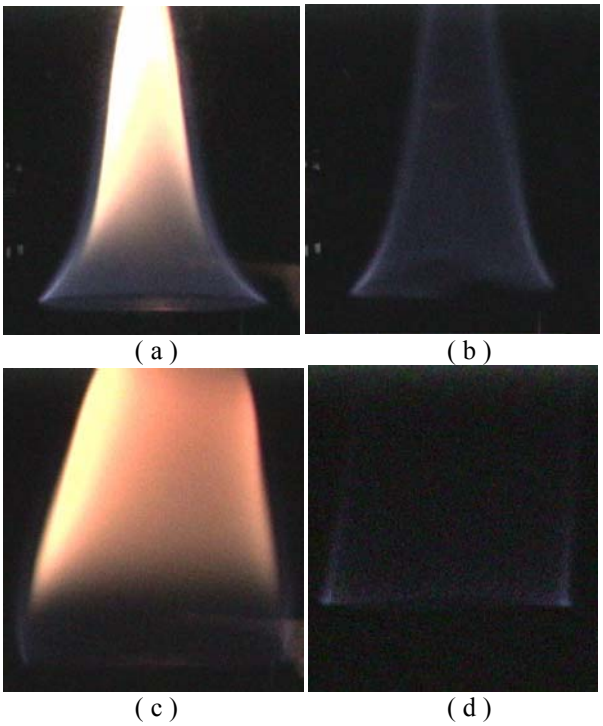

Fig. 2 Video images of cup-burner methane flames with or without agent (CO_2). (a)(b) 1*g*, U_f = 0.9 cm/s, U_o = 8.7 cm/s; (a) X_a = 0, (b) X_a = 0.16. (c)(d) μ*g*, U_f = 0.9 cm/s, U_o = 9.7 cm/s; (c) X_a = 0, (d) X_a = 0.215.

RESULTS AND DISCUSSION

Figure 2 shows video images of cup-burner flames of methane in air with or without agent (CO_2) in 1*g* and μ*g*. In 1*g* without agent (Fig. 2a), the blue flame base anchored at the burner rim with a steep inward inclination due to accelerating buoyancy-induced flow. Thus, the downstream portion of the flame was contracted and had an orange-yellow tip due to soot formation. The flame was dynamic (unstationary) due to flickering caused by instability of the buoyancy-induced flow. The flickering frequency measured at ≈5 cm above the burner by a photodiode was bimodal: ≈11 Hz or ≈15 Hz, depending on the air velocity. As CO_2 was added into the coflowing air (Fig 2b), the entire flame turned blue. As the CO_2 concentration was increased to the extinguishment limit, the flame base shifted gradually downstream and oscillated continuously before the flame blew off.

In μ*g* without agent (Fig 2c), the blue flame

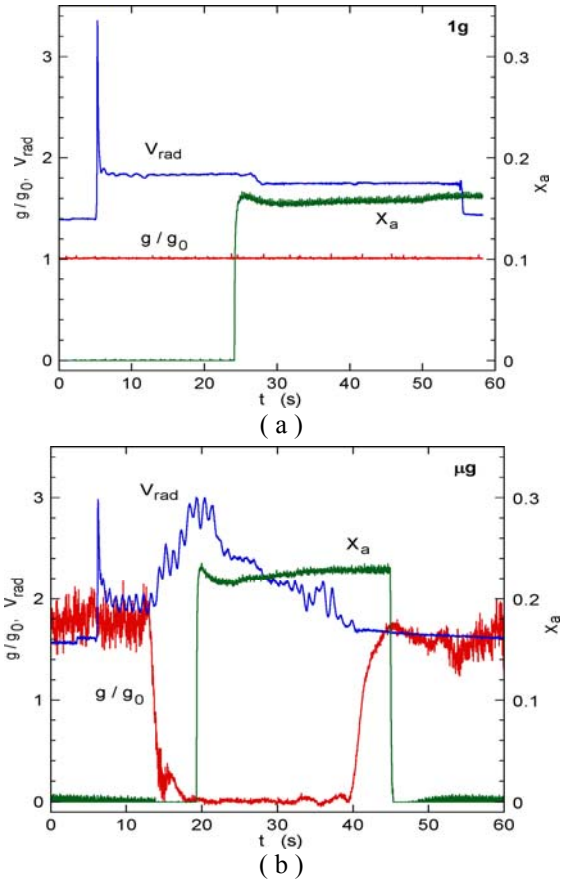

Fig. 3 Temporal variations of measured gravity level, radiometer output, and agent (CO_2) volume fraction. (a) 1*g*, (b) μ*g*.

attached to the outer edge of the burner rim and the downstream portion, including the yellow zone, expanded outwardly, thus making the flame fatter. As CO_2 was added (Fig 2d), the flame again turned blue. Furthermore, the flame zone was more upright, the downstream portion of the flame became very weak, and thus the flame tip appeared to be opened.

Figure 3 shows the measured *z*-axis gravitational acceleration (g), normalized by the earth gravity (g_0), radiometer output voltage (V_{rad}), and the agent (CO_2) volume fraction (X_a), determined from the air and agent flow rates. In 1g (Fig. 3a), the radiometer output showed a spike at ignition and then maintained a nearly constant level. The agent volume fraction showed an overshoot just after its introduction and then gradually increased as a manual metering valve was opened incrementally. Because there was a time lag between the agent volume fraction measurement and the actual time when the agent reached the flame location, the radiometer output level shifted down due to soot disappearance after approximately 4 ms after the agent release. Thus, the critical agent volume fraction at extinguishment was determined by taking into account the residence time of the oxidizer flow between the mixing point and the burner location.

Figure 3b shows the results of the aircraft experiment, during which the flame was ignited in the ~1.8g pull-up period, and the agent was released in the low-g period. The radiometer output increased as the gravity level dropped because the flame became larger (see Fig 2). The subsequent decrease in the radiometer output was due to continuous flame lifting and weakening above the burner until extinguishment.

Figure 4 shows the measured and calculated critical agent (CO_2) volume fraction at extinguishment (X_{ac}) as a function of the oxidizer velocity (U_o) in various environments at 1g. For air at 1 atm, the critical agent volume fraction was nearly independent of the oxidizer velocity over a wide range ($2 < U_o < 18$ cm/s). This insensitivity of the suppression limit to the oxidizer flow, once a minimum flow is achieved, (plateau region) has been reported in the literature[9,14,16]. The fuel velocity, the fuel cup diameter, and the chimney diameter are also known to have a small or negligible impact on the agent concentration at suppression[14]. In the plateau region, the current results of the X_{ac} measurement using the stainless-steel burner (○) was consistent with those obtained previously[25] with the standard glass burner (□). As the oxidizer velocity was decreased below the lower edge of the plateau region and approached a threshold ($U_o \approx 1$ cm/s) for forming an over-ventilated flame, X_{ac} decreased rapidly toward zero. Thus, an under-ventilated flame in $U_o < 1$ cm/s could never been stabilized on the burner. Decreasing the atmospheric pressure from 1 atm to 0.7 atm decreased X_{ac} only slightly. On the other hand, increasing the oxygen concentration in the oxidizer to 30 % doubled X_{ac} for both 1 and 0.7 atm. For 30 % O_2 and 1 atm, X_{ac} decreased slightly with increasing U_o.

Figure 5 shows the results of the extinguishment tests aboard the KC-135 and the calculated critical agent (CO_2) volume fraction at extinguishment in air at 0g. The low-g period during the parabolic flight (22 s

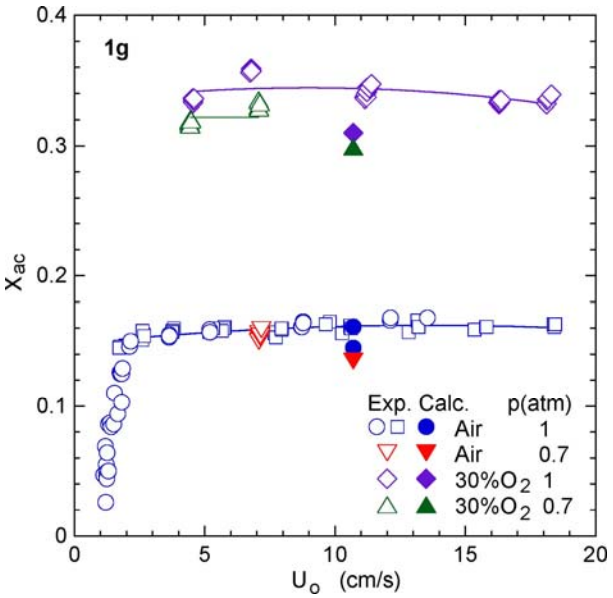

Fig. 4 Measured and calculated critical agent (CO_2) volume fraction at extinguishment in various oxidizing environments at 1*g*.

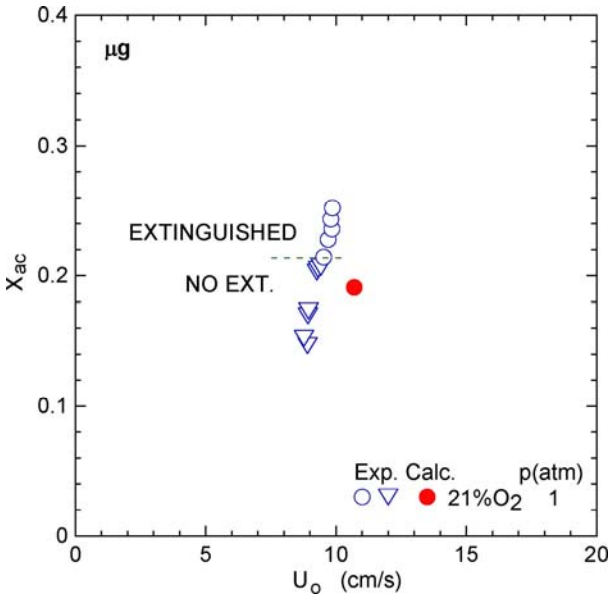

Fig. 5 Measured and calculated critical agent (CO_2) volume fraction at extinguishment in air at μ*g*.

to 25 s) was not long enough to reach the extinguishing concentration for the test, for which the initial agent concentration was too low. Figure 5 shows the data points for both extinguished and no extinguished tests. The MEC value was determined from the lowest extinguished data point.

Table 1 lists the experimental and calculated minimum extinguishing agent (CO_2) volume fractions, ($X_{ac,exp}$, $X_{ac,calc}$) as well as the corresponding limiting oxygen volume fractions ($X_{O2c,exp}$, $X_{O2c,calc}$) the heat capacity of the oxidizer ($C_{p,298,o}$), and the adiabatic flame temperature[31] (T_f) of the stoichiometric fuel-oxidizer mixture at the measured extinguishing condition for various oxidizing environments. The limiting oxygen volume fraction was converted from the extinguishing agent volume fraction as $X_{O2c} = X_{O2,initial}\ (1 - X_{ac})$, where $X_{O2,initial}$ = the initial oxygen volume fraction in the neat oxidizer. For 30 % O_2 environments, X_{ac} doubled, yet X_{O2c} was still higher, compared to the air cases. The calculated values were approximately 8 % lower, on average, than the measured values. Considering the complexity in the blowoff-type flame extinguishment processes as a result of interactions between chemistry and transport phenomena in the flow field in the flame stabilizing region, the predictions are in good agreement with the measurements. In fact, upper one of the two computed data points for the air, 1*g*, and 1 atm environment almost exactly matched the experiment. Only the differences in the computations were different kinetic parameters[32] for a methyl-H atom reaction step, $CH_3 + H + M \rightarrow CH_4 + M$, as described elsewhere[24].

Figure 6 shows the heat capacity of the oxidizer stream, and adiabatic flame temperature of a stoichiometric mixture of methane with the oxidizer, as a function of the CO_2 volume fraction; the measured extinguishment conditions in various oxidizing environments are shown by the points. Adding CO_2 has two effects: raising the heat capacity of the mixture ($C_{p,298,\,CO2}$ is 37.129 J/mol K whereas $C_{p,298}$ for N_2 or O_2 is about 29 J/mol K), and diluting the mixture, i.e., lowering the heat release per unit mass of oxidizer. The calculated adiabatic flame temperature accounts for these two effects, so that at the extinction point, T_f is decreased to the mid-1900s K (bounded by dashed lines) for all 1*g* flames as compared to neat oxidizers (air/1 atm, 2223 K; air/0.7 atm, 2214 K; 30 % O_2/1 atm, 2525 K; 30 % O_2/0.7 atm, 2506 K). This result indicates that the extinguishing CO_2 concentration was basically determined by the thermal and dilution effects. In microgravity, more agent concentration was required to extinguish the flame. Thus, the adiabatic flame temperature at the extinguishment condition was lowered to near 1800 K. The relatively high minimum extinguishing concentrations ($X_{ac} \geq 0.3$) for the 30 % O_2 environment suggest that in a practical sense, for these enriched oxygen environments, fire extinguishment and prevention of subsequent re-ignition is more difficult.

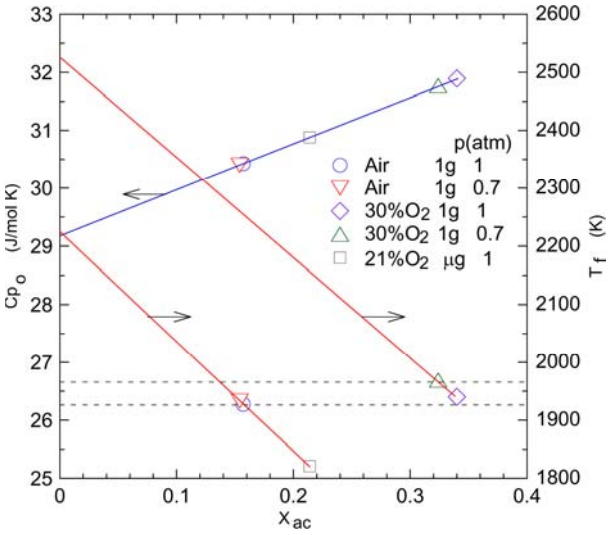

Fig. 6 Oxidizer heat capacity and adiabatic flame temperature at measured extinguishment limits in various oxidizing environments.

Table 1 Extinguishment limit, heat capacity, and adiabatic flame temperature.

Environment	$X_{ac,exp}$	$X_{ac,calc}$	$X_{O2c,exp}$	$X_{O2c,calc}$	$\frac{(X_{ac,calc} - X_{ac,exp})}{X_{ac,exp}}$	$C_{p,298,o}$ (J/mol K)	T_f (K)
Air/1*g*/1 atm	0.157	0.145, 0.161[a]	0.177	0.179, 0.176[a]	-0.076 0.025	30.43	1927
Air/1*g*/0.7 atm	0.154	0.135	0.178	0.181	-0.123	30.40	1933
30 % O_2/1*g*/1 atm	0.340	0.310	0.198	0.207	-0.088	31.90	1940
30 % O_2/1*g*/0.7 atm	0.324	0.299	0.203	0.210	-0.077	31.77	1969
21 % O_2/μ*g*/1 atm	0.214	0.191	0.165	0.170	-0.107	30.88	1815

[a] Using different kinetic parameters[32] for a methyl-H atom reaction step[24]

In the flame attachment and blowoff-type extinguishment processes typical of the cup burner, the flame structure near the flame base plays a decisive role. Figure 7 shows the calculated structure of a methane flame in the 30 % O_2 in N_2 mixture at 1*g*, including the velocity vectors (**v**), isotherms (*T*), total heat-release rate ($\dot{q}$), and the local equivalence ratio (ϕ_{local}). The local equivalence ratio is defined[33] by considering a stoichiometric expression for intermediate species in the mixture to be converted to CO_2 and H_2O and is identical to the conventional equivalence ratio in the unburned fuel-air mixture. The velocity vectors show the longitudinal acceleration in the hot zone due to buoyancy. As a result of the continuity of the fluid, surrounding air was entrained into the lower part of the flame. The entrainment flow inclined inwardly because of the minimal fuel flow rate. The heat-release rate contours showed a peak reactivity spot (i.e., the reaction kernel[19-21]) at the flame base. The heat-release rate, velocity, temperature, and local equivalence ratio at the reaction kernel were $\dot{q}_k$ = 193 J/cm^{3}s, $|v_k|$ = 0.224 m/s T_k = 1554 K, and ϕ_{local} = 0.95, respectively. Back diffusion of chain radical species into the oxygen rich incoming flow at the flame base (edge) enhanced the exothermic reactions, thus forming the reaction kernel. The reactivity decreased steeply in downstream portions of the flame (14 J/cm^{3}s at z = 5 mm) as this unique geometric feature of the edge diffusion flame was lost and the reactants were diluted by the combustion products, thus resulting in lower concentration gradients and then fluxes. On the other hand, the velocity increased downstream significantly (~3.2 m/s at z = 50 mm) by a cumulative effect of the buoyancy-induced flow. Thus, the vigorously burning reaction kernel sustained stationary combustion processes in the flow in the vicinity of the burner rim (flame attachment) and held the trailing diffusion flame as described in more detail elsewhere[19-21].

Figure 8 shows the variations of the species mole fractions (X_i), temperature, species formation rates ($\hat{\omega}_i$), and total heat-release rate across the reaction

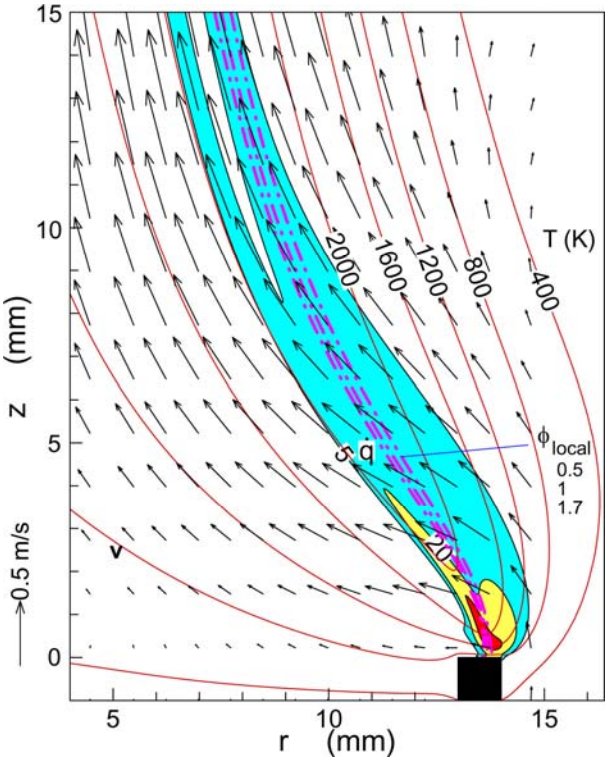

Fig.7 Calculated structure of a methane flame in 30%O_2 in N_2 mixture at 1*g*. $\dot{q}$ contours: 5, 20, and 80 J/cm^{3}s.

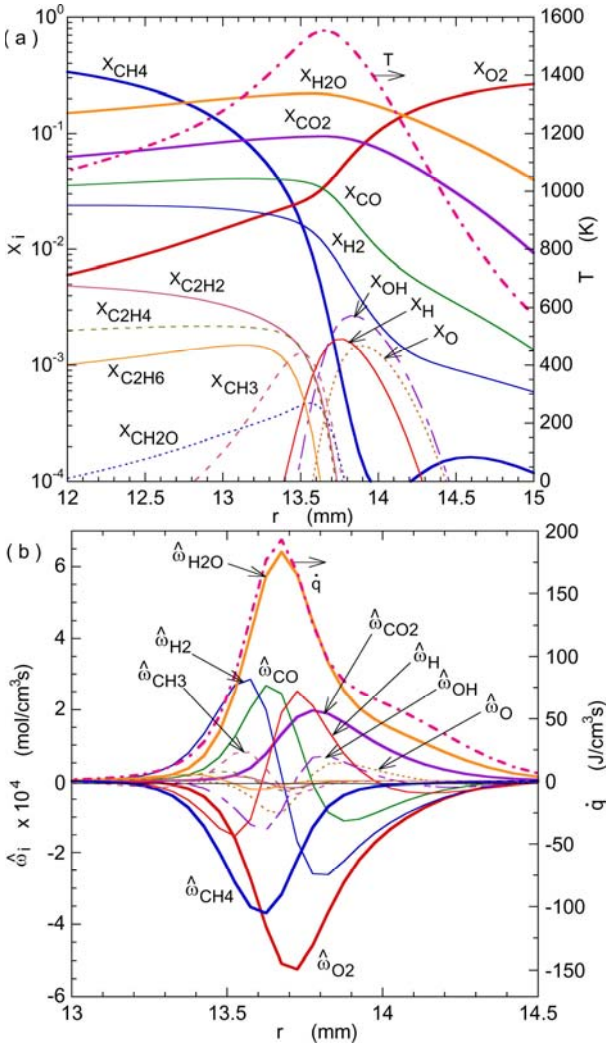

Fig. 8 Calculated variables across the reaction kernel of a methane flame in 30%O_2 in N_2 mixture at 1*g*. z_k = 0.48 mm. (a) Mole fractions, temperature, (b) production rate, and heat-release rate.

kernel of the uninhibited 1*g* flame in the 30 % O_2 in N_2 mixture. General trends in the species mole fractions and formation rates resembled to those in the cup-burner methane flame in air reported previously[26]. Basic features in the flame structure are typical of diffusion flames; i.e., chain radicals, formed at high temperatures on the air side (slightly) of the peak reaction zone, diffuse and dissociate the fuel into methyl, H_2 and CO and C_2 species (slightly) on the fuel side, and finally H_2 and CO are oxidized to the products on the air side. The heat-release rates of elementary steps (not shown) revealed that the methyl oxidation reaction, $CH_3 + O \rightarrow CH_2O + H$ (R19), and the final product formation, $H_2 + OH \rightarrow H_2O + H$ (R165), were major contributors to the total heat-release rate peak. The reaction rates of elementary steps (not shown) indicated that the chain-branching, $H + O_2 \rightarrow OH + O$ (R73), was the fastest reaction of all, with its peak reaction rate coincident with the heat-release rate peak. Other fast reactions were the fuel dehydrogenation, $CH_4 + OH \rightarrow CH_3 + H_2O$ (R191) and $CH_4 + H \rightarrow CH_3 + H_2$ (R103), on the fuel side, the methyl oxidation (R19) at the heat-release rate peak, and the final product formation, (R165) and $CO + OH \rightarrow CO_2 + H$ (R193) on the air side.

Figure 9 shows the calculated structure of a near-extinguishment-limit 1*g*-flame in the 30 % O_2 in N_2 mixture with 30.9% CO_2 added to the oxidizer. The flame base detached from the burner rim and shifted inwardly above the burner. The incoming flow into the reaction kernel was almost horizontal. The flame base oscillation just prior to extinguishment was reported previously[25] for air. The heat-release rate, velocity, temperature, and local equivalence ratio at the reaction kernel were $\dot{q}_k = 151$ J/cm^{3}s, $|v_k| = 0.246$ m/s $T_k = 1479$ K, and $\phi_{local} = 0.64$, respectively. As a result of CO_2 addition, the reaction-kernel temperature (and the heat-release rate) decreased mildly. By contrast, the flame temperature in the trailing diffusion flame (not shown) decreased nearly 500 K (from 2160 K to 1668 K at z = 10 mm), which was nearly equal to the reduction in the

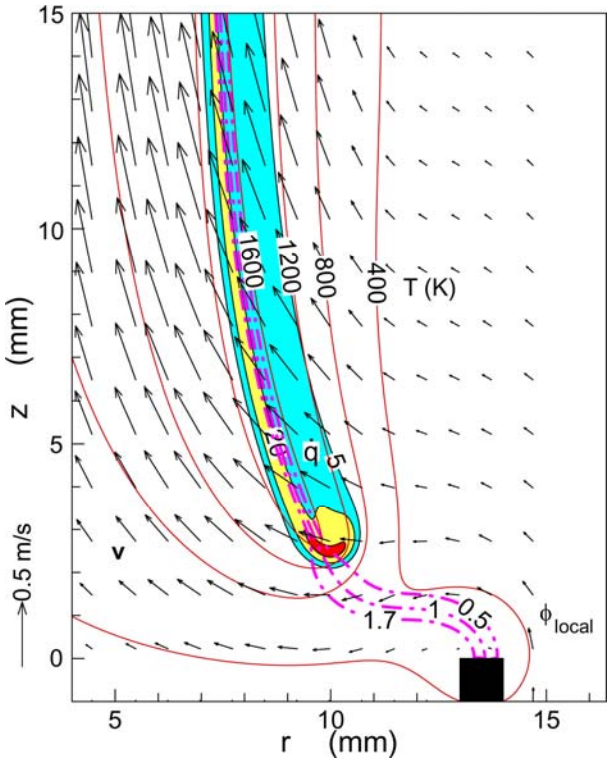

Fig. 9 Calculated structure of a methane flame in 30%O_2 in N_2 mixture with 30.9% added CO_2 at 1*g*. $\dot{q}$ contours: 5, 20, and 80 J/cm^{3}s.

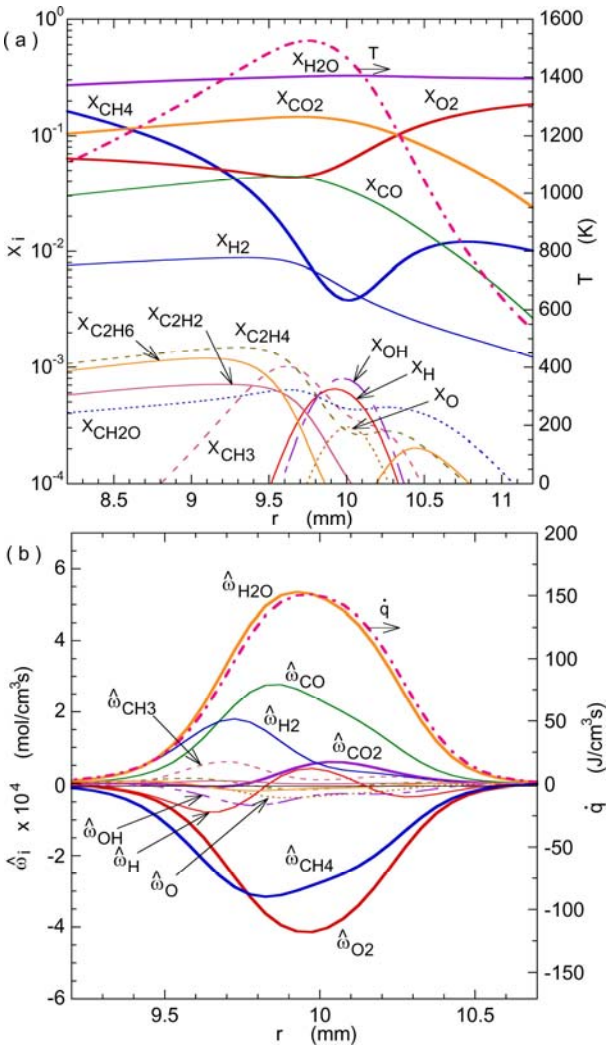

Fig. 10 Calculated variables across the reaction kernel of a methane flame in 30%O_2 in N_2 mixture with 30.9% added CO_2 at 1*g*. z_k = 2.48 mm. (a) Mole fractions, temperature, (b) production rate, and heat-release rate.

adiabatic flame temperature (Fig. 7).

Figure 10 shows the variations of calculated variables across the reaction kernel of the 1*g* flame in the 30 % O_2 in N_2 mixture with 30.9% CO_2 added to the oxidizer. The CO_2 addition reduced the oxygen concentration in the oxidizer down from 30 % to 20.7 % (Table 1), i.e, dilution effect. The mole fractions and formation rates of chain radicals (OH, H, and O) decreased significantly. Nevertheless, the reaction kernel was still vigorously burning just prior to extinguishment, thus supporting the much weaker trailing flame zone. Thus, the cup-burner extinguishment phenomenon is neither due to global extinction of the diffusion flame nor local extinction at the reaction kernel. It is rather due to continuous flame stabilization processes to search a new balancing point in the flow in response to an increase in the agent concentration.

Figure 11 shows the calculated structure of a methane flame in the 30 % O_2 in N_2 mixture at 0*g*. The heat-release rate, velocity, temperature, and local equivalence ratio at the reaction kernel were $\dot{q}_k = 260$ J/cm^{3}s, $|v_k| = 0.257$ m/s $T_k = 1477$ K, and $\phi_{local} = 0.90$, respectively. General features of the flame are similar to the coflow methane-air 0*g*-flames previously studied using the cup-burner[26] and a small tube burner[21].

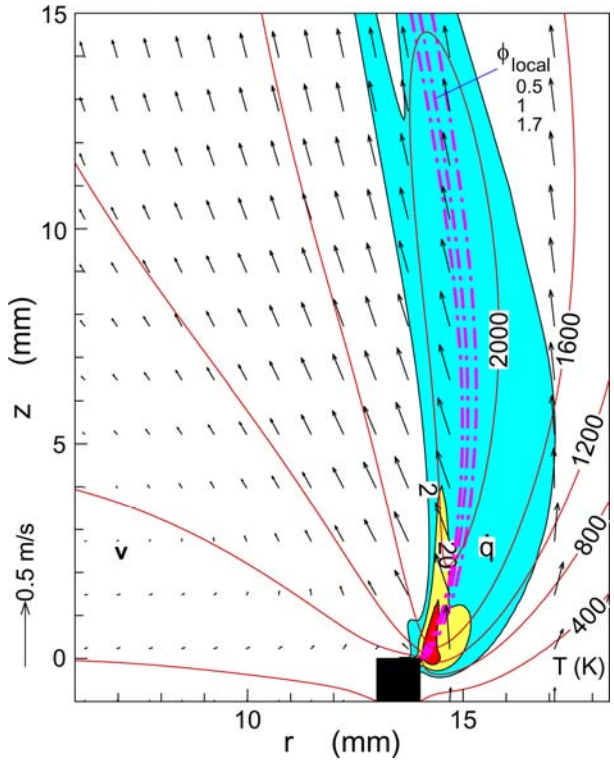

Fig. 11 Calculated structure of a methane flame in 30%O_2 in N_2 mixture at 0*g*. $\dot{q}$ contours: 2, 20, and 80 J/cm^{3}s.

Because of lack of buoyancy, the velocity vectors show only slight acceleration in the hot zone due to thermal expansion. As the momentum of the coflowing air transferred to the low-speed wake-like region behind the cup burner, the velocity distribution became nearly uniform downstream. The flame zone was formed nearly vertically, and the surrounding air came into the lower part of the flame. Figure 13 shows the variations of the calculated variables across the reaction kernel of the 0*g* flame. The flame structure was similar to that of the 1*g* flame (Fig. 7), except that the 0*g* flame was somewhat more reactive and the heat-release rate was larger at the reaction kernel. The heat-release rate decreased rapidly downstream in the same manner with the 1*g* attached flame (Fig. 7) and became very small

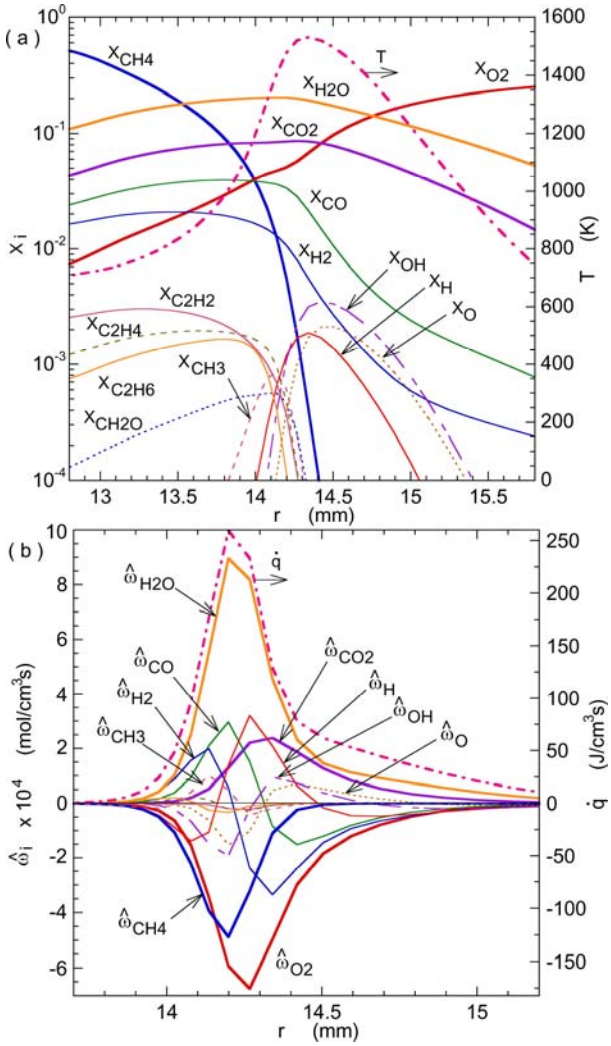

Fig. 12 Calculated variables across the reaction kernel of a methane flame in 30%O_2 in N_2 mixture at 0*g*. z_k = 0.18 mm. (a) Mole fractions, temperature, (b) production rate, and heat-release rate.

because the velocity stayed at a low level (~0.22 m/s), thus resulting in low species concentration gradients and fluxes. As a result, the downstream portion of the 0*g* flame was much weaker than that of the 1*g* flame.

Figure 13 shows the calculated structure of a near-extinguishment-limit 0*g*-flame in the 30 % O_2 in N_2 mixture with 33% CO_2 added to the oxidizer. The high CO_2 mole fraction shows the highly diluted reaction zone. The heat-release rate, velocity, temperature, and local equivalence ratio at the reaction kernel were $\dot{q}_k$ = 78.1 J/cm^{3}s, $|v_k|$ = 0.142 m/s T_k = 1424 K, and ϕ_{local} = 0.61, respectively. The gas velocity increases in the hot zone due to thermal expansion and is directed toward the low-speed wake behind the cup burner, thus forming a recirculation zone. The fuel-oxidizer mixing occurred over the stand-off distance of ≈6 mm, which converts to the residence time of ≈0.06 s. The heat-release rate contours show a hook-shaped flame base with the reaction kernel, which resembles to that in jet diffusion flames in coflowing air in 1*g* studied previously[20]. The flame tip opened as the extinction of the trailing flame occurred as the heat-release rate decreased downstream and radiative heat losses became substantial (~37% at z = 10 mm).

Figure 14 shows the variations of the calculated variables across the reaction kernel of the near-limit 0*g* flame. The flame structure resembled the near-limit 1*g* flame (Fig. 10), except that the reaction rates and heat-release rate halved. As a result of the vigorously burning reaction kernel inside the incoming flammable mixture flow, the radial distributions of the species mole fractions show a unique flame structure, where the fuel-side variations are somewhat mirrored on the air side with the leftover fuel. This trend was also observed previously[33] in the edge diffusion flame propagating through the flammable mixture layer in the fuel jet.

The practical relevance of the current findings to space fire suppression is the fact that fire spread over condensed fuel surfaces and extinguishment of such fires relate to the attachment and blowoff processes of edge diffusion flames as represented by the cup-burner

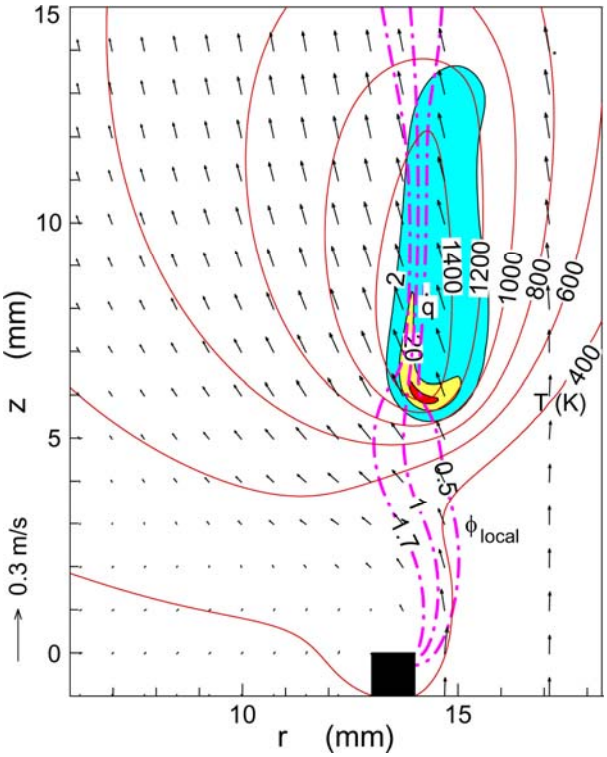

Fig. 13 Calculated structure of a methane flame in 30%O_2 in N_2 mixture with 33% added CO_2 at 0*g*. $\dot{q}$ contours: 2, 20, and 80 J/cm^{3}s.

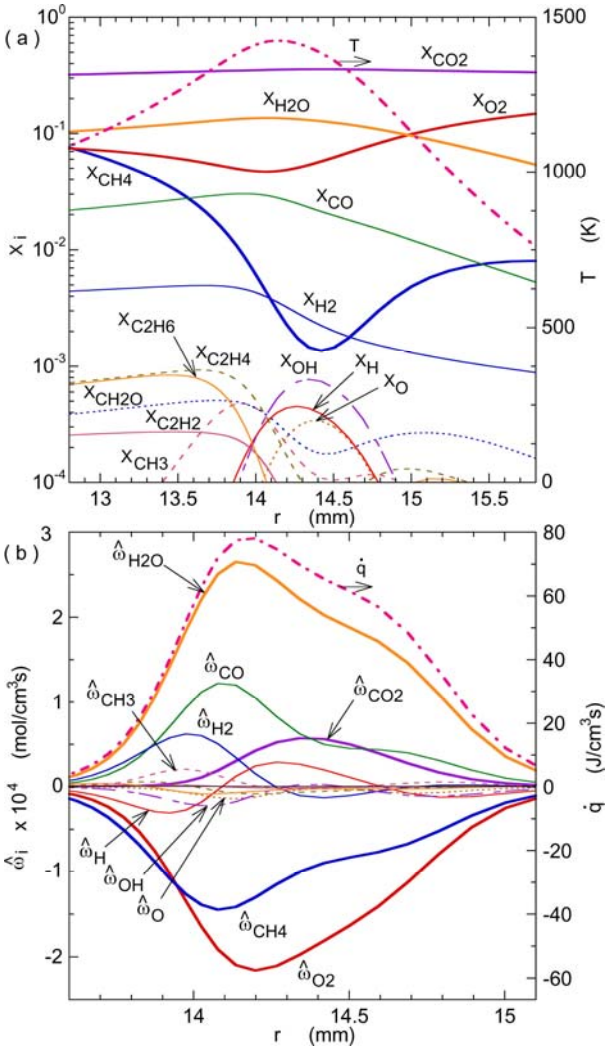

Fig. 14 Calculated variables across the reaction kernel of a methane flame in 30%O_2 in N_2 mixture with 33% added CO_2 at 0*g*. z_k = 5.93 mm. (a) Mole fractions, temperature, (b) production rate, and heat-release rate.

flame. During the blowoff process of 0*g* flames caused by dilution with the inert gas, the reaction-kernel temperature decreased moderately, whereas the velocity and the heat-release rate decreased more substantially. This result suggests that the reaction kernel shifted downstream to seek a location where the residence time (which depends on the reciprocal of the velocity) is sufficient for the longer chemical reaction time (which depends on the reciprocal of the reactivity) caused by dilution (lower oxygen concentration). Therefore, the overall mechanism of the flame-base movement is based on the subtle balance between the chemical time and the residence time at the reaction kernel, not the trailing diffusion flame. This reaction kernel hypothesis [19-21] has been proposed for the lifting process of jet diffusion flames as a result of an increase in the coflowing air velocity. A main difference is that, unlike the dilution process, increasing the coflowing air velocity increased the peak reactivity (the "blowing effect") and pushed further the reaction-kernel downstream at higher velocities.

CONCLUSIONS

The laboratory and aircraft experiments and numerical simulations with full chemistry have revealed the flame structure and extinguishment behavior of laminar methane diffusion flames in co-flowing normal or oxygen-enriched air in the cup-burner configuration under 1*g* and 0*g* conditions. In 1*g*, the buoyancy-induced flow acceleration in the hot region downstream resulted in the inward air entrainment into the wake behind the cup burner, thus inclining the burner-rim-attached edge diffusion flame inwardly. As the agent (CO_2) was added to the oxidizer, the flame base detached and pushed inwardly above the burner toward the more squeezed flow zone in search of a new stabilizing point. By contrast, in 0*g*, the attached flame zone was upright due to lack of buoyancy-induced flow and detached axially downstream at relatively low velocities with the tip of the flame opened due to extinction in the downstream portion by radiative heat losses. In both 1*g* and 0*g*, the reaction kernel (a peak reactivity spot) at the edge diffusion flame is responsible for both the trailing diffusion flame holding and extinguishment via blowoff processes.

The minimum extinguishing concentrations of CO_2 doubled in the 30 % O_2 in N_2 mixture compared to those in air at 1 atm and 0.7 atm in 1*g* tests. The MEC of CO_2 in air at μ*g* was ~36 % higher than that in 1*g*. Further aircraft testing is needed for oxygen-enriched conditions. Fire suppression for space fires would become practically difficult if the MEC value approached to 40 %.

ACKNOWLEDGMENT

This research was supported by the Office of Biological and Physical Research, National Aeronautics and Space Agency, Washington, D.C. Assistance by Philip Werk, Benjamin Chan (Case Western Reserve University), David Bennett (Akima Corporation), and Mike Jamison (ZIN Technologies) in conducting the experiment is acknowledged.

REFERENCES

1. Friedman, R., Fire Safety in Extraterrestrial Environments, NASA/TM-1998-207417, 1998.
2. Friedman, R., Fire Safety in the Low-Gravity Spacecraft Environment, NASA/TM-1999-209285, 1999.
3. Friedman, R., and Ross, H. D., Combustion Technology and Fire Safety for Human-crew Space Missions, In *Microgravity Combustion: Fire in Free Fall* (H. D. Ross Ed.), Academic Press, San Diego, 2001, p.83.
4. Williams, F.A., *J. Fire Flammability* 5:54 (1974).
5. Sheinson, R. S., Pener-Hahn, J. E., and Indritz, D., The Physical and Chemical Action of Fire Suppressants, *Fire Safety Journal,* 15, 437-450 (1989).
6. Grosshandler, W. L., Gann, R. G., and Pitts, W. M., (eds.), Evaluation of Alternative In-Flight Fire Suppressants for Full-Scale Testing in Simulated Aircraft Engine Nacelles and Dry Bay, SP 861, National Institute of Standards and Technology, 1994.
7. Harrison, G. C., Halon Replacement in Aircraft and Industrial Applications, In *Halon Replacements: Technology and Science* (A. W. Miziolec and W. Tsang, Eds.), American Chemical Society, Washington, DC, 1995, pp. 74-84.
8. Annon., Workshop on Research for Space Exploration: Physical Sciences and Process Technology, NASA/CP-1998-207431, May 1998.
9. Annon., "Standard on Clean Agent Fire Extinguishing Systems," National Fire Protection Association, NFPA 2001, Quincy, MA, 2000.
10. Annon., "Gaseous Fire-Extinguishing Systems—Physical Properties and System Design," International Organization for Standardization, ISO 14520-Part I, 2000.
11. Bajpai, S. N., "An Investigation of the Extinction of Diffusion Flames by Halons," Journal of Fire and Flammability 5: 255 (1974).
12. Hirst, R., and Booth, K., "Measurements of Flame-Extinguishing Concentrations," Fire Technology 13: 4 (1977).
13. Sakai, R., Saito, N., Saso, Y., Ogawa, Y., and Inoue, Y., Flame Extinguishing Concentrations of Halon

Replacements for Flammable Liquids, Report of Fire Research Institute of Japan, No. 80, 1995, pp. 36-42.
14. Hamins, A., Gmurczyk, G., Grosshandler, W., Rehwoldt, R. G., Vazquez, I., Cleary, T., Presser, C., and Seshadri, K., "Flame Suppression Effectiveness," Evaluation of Alternative In-Flight Fire Suppressants for Full-Scale Testing in Simulated Aircraft Engine Nacelles and Dry Bays (W. L. Grosshandler, R. G. Gann, and W. M. Pitts, Eds.), National Institute of Standards and Technology, NIST SP 861, Gaithersburg, MD, 1994, pp. 345-465.
15. Linteris, G.T. and Gmurczyk, GW., "Prediction of HF Formation During Suppression," in Fire Suppression System Performance of Alternative Agents in Aircraft Engine and Dry Bay Laboratory Simulations (R.G. Gann, Ed.), National Institute of Standards and Technology, NIST SP 890: Vol. II, Gaithersburg, MD, 1995, pp. 201-318.
16. Moore, T. A., Martinez, A., and Tapscott, R. E., "A Comparison of the NMERI and ICI-style Cup-Burners," Proceedings of the 7th Halon Options Technical Working Conference (HOTWC-97), Albuquerque, NM, 1997, pp. 388-395.
17. Saito, N., Ogawa, Y., Saso, Y., and Sakai, R., "Improvement on Reproducibility of Flame Extinguishing Concentration Measured by Cup Burner Method," Report of Fire Research Institute of Japan, No. 81, 1996, pp. 22-29.
18. Senecal, J. A., "Flame Extinguishing by Inert Gases: Theoretical & Experimental Analysis," Proceedings of the 2004 Spring Technical Meeting of the Central States Section of the Combustion Institute, March 2004.
19. Takahashi, F., Schmoll, W. J., and Katta, V. R., "Attachment Mechanisms of Diffusion Flames," Proceedings of The Combustion Institute, Vol. 27, 1998, pp. 675-684.
20. Takahashi, F., and Katta, V. R., "A Reaction Kernel Hypothesis for the Stability Limit of Methane Jet Diffusion Flames," Proceedings of The Combustion Institute, Vol. 28, 2000, pp. 2071-2078.
21. Takahashi, F., and Katta, V. R., "Reaction Kernel Structure and Stabilizing Mechanisms of Jet Diffusion Flames in Microgravity," Proceedings of The Combustion Institute, Vol. 29, Pittsburgh, PA, 2002, pp. 2509-2518.
22. Katta, V. R., Takahashi, F., and Linteris, G. T., "Numerical Investigations of CO_2 as Fire Suppressing Agent," Fire Safety Science: Proceedings of the Seventh International Symposium, International Association for Fire Safety Science, 2003, pp. 531-544
23. Katta, V. R., Takahashi, F., and Linteris, G. T., "Suppression of Cup-Burner Flames Using Carbon Dioxide in Microgravity," Combustion and Flame 137, 506-522 (2004).
24. Linteris, G. T., Katta, V. R., and Takahashi, F., "Experimental and Numerical Evaluation of Metallic Compounds for Suppressing Cup-Burner Flames," Combustion and Flame 138, 78-96 (2004).
25. Takahashi, F., Linteris, G., and Katta, V. R., "Suppression of Cup-Burner Flames," Fourth International Symposium on Scale Modeling (ISSM-IV), Cleveland, OH, September 2003.
26. Takahashi, F., Linteris, G., and Katta, V. R., "Suppression Characteristics of Cup-Burner Flames in Low Gravity," AIAA 42nd Aerospace Sciences Meeting, Paper No. 2004-0957, Reno, Nevada, January 2004.
27. Roquemore, W. M., and Katta, V. R., Role of Fow Visualization in the Development of UNICORN, *Journal of Visualization*, Vol. 2, No. 3/4, 257-272 (2000).
28. Frenklach, M., Wang, H., Goldenberg, M., Smith, G. P., Golden, D. M., Bowman, C. T., Hanson, R., K., Gardiner, W. C., and Lissianski, V., GRI-Mech—An Optimized Detailed Chemical Reaction Mechanism for Methane Combustion, Technical Report No. GRI-95/0058, Gas Research Institute, Chicago, Illinois, 1995.
29. Annon., Radiation Models, International Workshop on Measurement and Computation of Turbulent Nonpremixed Flames., http://www.ca.sandia.gov/TNF/radiation.html, 2003.
30. Katta, V. R., Goss, L. P., and Roquemore, W. M., Numerical Investigatios of Transitional H_2/N_2 Jet Diffusion Flames, *AIAA Journal,* 32, 84 (1994).
31. McBride, B. J., and Gordon, S., Computer Program for Calculation of Complex Chemical Equilibrium Compositions and Applications—II. Users Manual and Program Description, NASA Reference Publication 1311, June 1996.
32. Warnatz, J., in *Combustion Chemistry* (W. C. Gardiner, ed.), Springer-Verlag, New York, 1984, pp. 197-360.
33. Takahashi, F., and Katta, V. R., "Structure of Propagating Edge Diffusion Flames in Hydrocarbon Fuel Jets," Proceedings of The Combustion Institute, Vol. 30, Pittsburgh, PA, 2004, in press.